

# Transforming static trusses into shape morphing systems using principles of quadrilateral linkages

Hardik Y. Patil<sup>a,1</sup>, Evgueni T. Filipov<sup>a,b,\*</sup>

<sup>a</sup>*Civil and Environmental Engineering, University of Michigan, Ann Arbor, 48109, Michigan, USA*

<sup>b</sup>*Mechanical Engineering, University of Michigan, Ann Arbor, 48109, Michigan, USA*

---

## Abstract

Trusses are valued for their simple design principles and efficient load-bearing capability. However, their slow assembly process and static topology restrict rapid deployment and reconfiguration for functional use. Mechanical linkages, in contrast, offer rapid deployability and reconfigurability but are challenging to apply as large-scale civil structures. These challenges raise the question: Can the design versatility of trusses be combined with the kinematic advantages of mechanical linkages to create structurally efficient, deployable, and reconfigurable large-scale systems? To that end, we present a method inspired by flat-foldable quadrilateral linkages to transform static trusses into compactly stowable, reconfigurable systems. An additional node is introduced on the tensile members of triangular units based on Grashof linkage principles. This node converts triangles into flat-foldable quadrilateral linkages, enabling system-level reconfigurability while preserving the load capacity, stiffness and stability of the structure. We show that the Fink, Scissor, and Warren trusses can be transformed into reconfigurable systems, achieving up to 93% and 60% reduction in convex hull area and maximum length, respectively, upon actuation of all degrees of freedom. Our method also extends to topology-optimized trusses, enabling the design of functional, shape-morphing trusses for arbitrary geometries, loads, and support conditions. Proof-of-concept prototypes, including a reconfigurable cantilever and a three-meter Warren truss bridge, validate feasi-

---

\*Corresponding author at:

Email address: filipov@umich.edu (Evgueni T. Filipov)

<sup>1</sup>First author

<sup>2</sup>DISTRIBUTION STATEMENT A. Approved for public release; distribution is unlimited. OPSEC9589.

bility while demonstrating load capacities and stiffness comparable to their static counterparts. We believe the proposed method will advance the design, analysis and fabrication of sophisticated bar-linked reconfigurable structures with potential applications in deployable infrastructure, aerospace systems, robotic components, consumer devices, metamaterials, and more.

*Keywords:* Reconfigurable trusses, Shape-morphing trusses, Foldable trusses, Four-bar linkages

---

## 1. Background on reconfigurable trusses

Trusses embody a simple yet efficient engineering concept of arranging material in a network of triangles to create stable, load-bearing structures. This simplicity has made trusses a preferred solution for supporting large loads for around 5000 years. The earliest occurrence of trusses dates back to the third-millennium BCE (Farshad and Isfahanian, 1978) when timber trusses were employed to support grain storage and other agricultural activities. Over centuries, truss designs have evolved to find new forms and applications with the adoption of new materials, analysis methods and construction techniques. The transition from timber to iron and steel trusses (Thorne, 2017; Gasparini and Provost, 1989), coupled with advancements in analytical and finite element methods (Hibbeler and Tan, 2006; Turner et al., 1956; Clough, 1960), has enabled precise sizing of members to make trusses more efficient at carrying loads. Furthermore, modern computational tools such as topology optimization (Stolpe, 2016) have enabled engineers to design and construct increasingly complex truss structures to accommodate any geometry, load, or support conditions. Despite these advances, modern trusses lack reconfigurability. The slow member-by-member assembly process of trusses prevents rapid deployment, while their static topology restricts shape-morphing for functional use. Once constructed, trusses serve a single purpose and require complete dismantling for relocation, limiting adaptability and compact storage for transport. These limitations underscore the need for innovative designs that introduce reconfigurability in truss structures without compromising structural integrity.

The need for reconfigurable systems for functional use has motivated extensive research into various bar-linked mechanical linkages. One well-studied example is the Scissor linkage (You and Pellegrino, 1997). This linkage utilizes straight or angulated rods to form tessellations of parallel-

ograms, enabling transformations along linear (Kim et al., 2021), radial (Patel and Ananthasuresh, 2007) and spherical (Hoberman, 1991) paths. Scissor linkages have been employed in a variety of applications, including deployable bridges (Ario et al., 2013), retractable arches (Brouwer, 2002; Mira et al., 2014), retractable roofs (Kassabian et al., 1999), and support structures for space antennas (Han et al., 2019). Beyond Scissor mechanisms, overconstrained linkages such as the Bricard (Baker, 1980), Myard (Liu and Chen, 2009) and Bennett (Chen and You, 2005) linkages have been utilized to design large mobile structures by tessellating individual unit cells. These linkages have been proposed for large-scale applications, including a deployable mesh-reflector antenna (Qi et al., 2017). Another class of reconfigurable structures is tensegrity (Snelson, 1965), which utilizes the equilibrium of compressive bars and tensile cables to create lightweight, deployable space masts (Tibert, 2002), robots (Liu et al., 2022) and more. Bar linkages have also been explored to design mechanisms capable of polyhedral scaling (Kiper et al., 2008). Furthermore, optimization techniques have helped achieve desired kinematic behavior and deployed shapes while ensuring adequate structural performance (Li and Krishnan, 2023). Some studies have also investigated topology optimization of bar-linkages (Kim and Kim, 2014) and the feasibility of generating various deployed shapes using single element type (García-Mora and Sánchez-Sánchez, 2021). A wide array of bar-linked mechanisms now enable the design of reconfigurable systems for diverse applications. However, most design approaches begin by developing a deployable unit or component, which is then assembled into a larger system. While this bottom-up approach has proven effective, the overall system behavior is often constrained by the characteristics and limitations of its fundamental unit.

In contrast, starting with a desired static bar-linked structure and modifying its members to incorporate a mechanism for reconfigurability offers broader design possibilities for designing deployable systems. One such approach involves replacing rigid truss members with telescoping beams. This approach has enabled the one-dimensional deployable truss to achieve linear transformation (Miura, 1984) and the shape-morphing hinged truss to exhibit bending and twisting (Sofla et al., 2009). However, the transformation limits of telescopic beams often constrain overall reconfigurability. In cases where large motion is achieved, the manual release of locks to allow telescoping reduces deployment efficiency. Others have explored substituting truss bars with

scissor linkages (Wang et al., 2015) and tensile members with cables (Giersch and Knarr, 2010) to enable structural transformations. While promising, these approaches often introduce complex gear-driven joints and actuators, increasing fabrication challenges. Yao et al. (2023) presents an example of the decomposition of triangular truss units into linkages by integrating semi-rigid joints that permit reconfigurability. A similar concept is seen in the Heatherwick Rolling Bridge (Studio, 2002; Packman, 2005), which incorporates hydraulic actuator supported hinges for structural reconfiguration. However, these existing approaches to decompose truss units represent isolated cases and lack a generalised workflow that can be applied to a broad range of truss structures. This gap highlights the need for a systematic method to transform static trusses into deployable, scalable and efficient reconfigurable systems.

To that end, this paper aims to introduce a general workflow that converts static trusses with a series of triangles into foldable, reconfigurable systems. The proposed workflow leverages the concepts of quadrilateral linkages (Barker, 1985) to strategically introduce an additional node within each triangular unit of a given truss. The placement of these nodes is guided by the flat-foldability criterion for planar Grashof quadrilateral linkages, the geometry of the triangular unit, and the force characteristics of the truss members. Using this workflow, we demonstrate the transformation of different conventional truss designs into reconfigurable systems, showcasing their theoretical capacity for flat-folding and analysing their kinematic behavior. Additionally, we illustrate how this approach is generalizable and can be applied to topology-optimized trusses, producing reconfigurable trusses with arbitrary geometries. Lastly, we show that the proposed reconfigurable trusses not only enable shape morphing but also ensure that the structure maintains its load capacity and structural stiffness by fabricating proof-of-concept prototypes. The method proposed in this work is available as an open-source code described Section 8.

The remainder of the manuscript is organised as follows. Section 2 presents the methodology for transforming a static truss into a reconfigurable system. This section outlines the criteria for node placement in triangular units of a truss and a workflow for achieving system-level reconfigurability. Next, Section 3 applies the proposed method to three traditional truss designs. Here, we demonstrate the ability to transform conventional trusses into reconfigurable systems and assess the kinematic behavior of the trusses upon the sequential actuation of their kinematic

degrees of freedom. The kinematic behavior of reconfigurable trusses is simulated using a sequential kinematic analysis program outlined in Appendix A. Section 4 extends the proposed method to topology-optimized trusses with arbitrary geometries. The subsections explain post-processing steps for topology-optimized trusses and kinematic analysis of three reconfigurable topology-optimized trusses. Next, Section 5 describes fabrication strategies for efficient shape-morphing behavior and demonstrates the structural behavior of proof-of-concept reconfigurable truss prototypes. Section 6 discusses the key contributions and limitations of the proposed method, with a commentary on potential topics for future work. Finally, concluding remarks are presented in Section 7.

## 2. Transforming static triangulated trusses into reconfigurable systems

In this section, we detail the process of transforming triangular elements into reconfigurable quadrilateral linkages by introducing an additional node. We also outline a workflow based on the geometric and force-based criteria for the node placement to achieve system-level reconfigurability.

### 2.1. *From triangles to reconfigurable quadrilateral linkages*

A triangle is the only polygonal shape that cannot be deformed without changing the length of its sides. This unique property endows triangles with exceptional structural rigidity, making them a fundamental element in the design of truss structures. However, traditional trusses are static, and there is an ever-increasing demand for reconfigurable structures that morph their shape to serve diverse purposes. To transform a static truss into a reconfigurable system, we propose a method of transmuting the triangular units of a truss into quadrilateral linkages (Barker, 1985) by introducing an additional node. This additional node is introduced such that the resulting quadrilateral linkage satisfies the Grashof condition. According to the Grashof condition (Grashof, 1883), the linkage will permit full rotation of the shortest link with respect to the adjacent links if the sum of the shortest (S) and the longest (L) links is less than or equal to the sum of the other two links (P & Q). Furthermore, the linkage can be reconfigured to fold flat and achieve a maximum reduction in

its convex hull area when the node placement fulfils the *flat-foldability criterion*, expressed as:

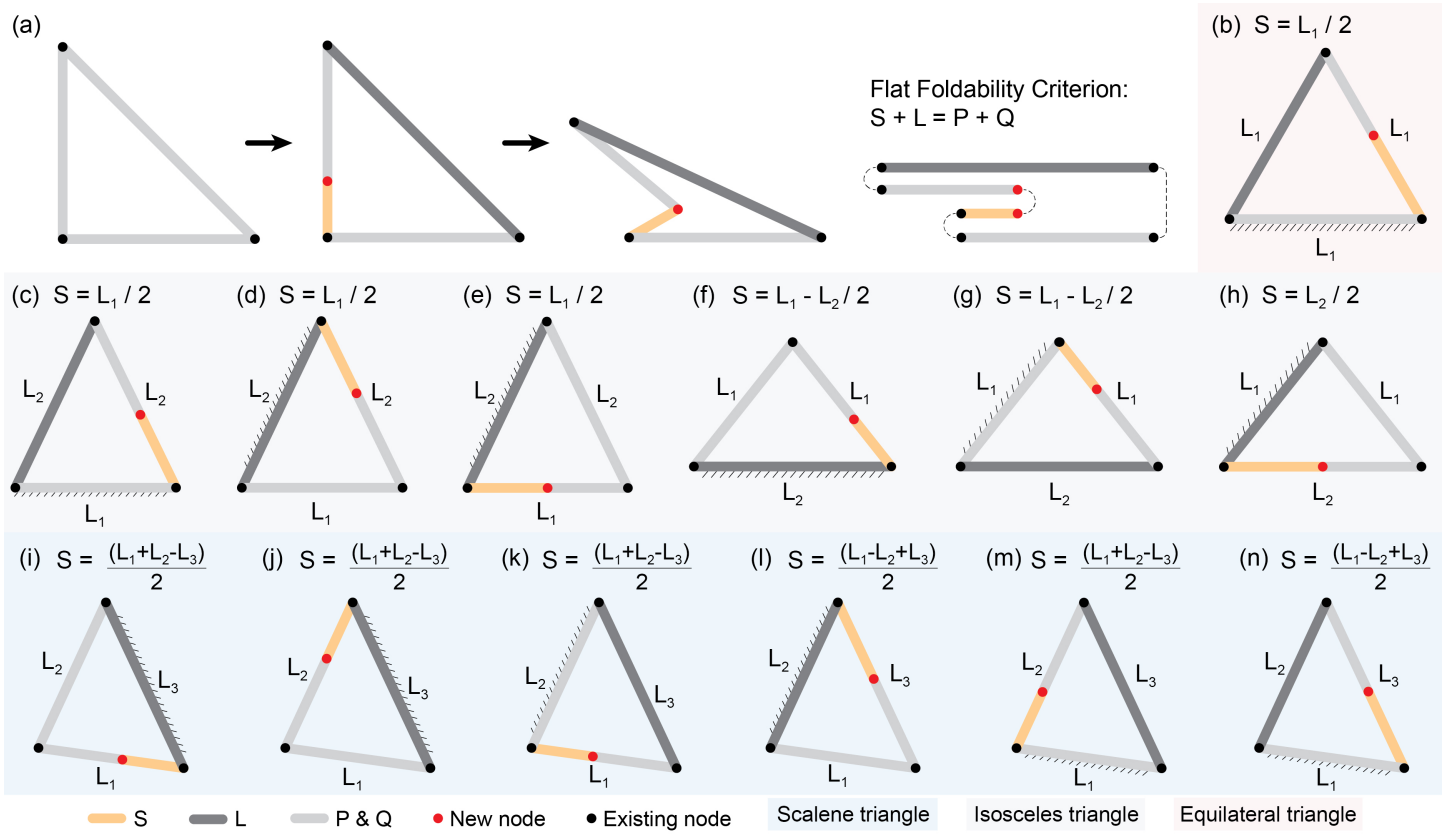
$$S + L = P + Q. \quad (1)$$

Figure 1 (a) demonstrates the proposed method of transmuting a triangle into a flat-foldable quadrilateral linkage, also known as a Grashof linkage that fulfils the flat-foldability criterion.

## 2.2. Rules for determining node location in an individual triangle

The precise location of the newly introduced node is determined based on the lengths of the members forming the triangular unit. In our method, the member of the triangular unit that remains fixed relative to the moving links in the resulting quadrilateral linkage is called the Ground link, while the member decomposed by adding a node is called the Candidate link. We introduce a new node that splits the Candidate link into two links. The link adjacent to the Ground link is made the shortest link  $S$ . The length  $S$  is derived such that the four links formed after the introduction of the node comply with the flat-foldability criterion discussed in Section 2.1, such that the linkage can fold flat with respect to the Ground link. It is important to note that the orientation of the  $S$ ,  $L$ ,  $P$  and  $Q$  links in the formed quadrilateral linkage is interchangeable and does not affect flat-foldability as long as the condition  $S + L = P + Q$  is met. However, to keep things simple and consistent, we ensure that the smallest link  $S$  is always positioned next to the Ground link. The formulae to determine length  $S$  based on the side lengths of the triangle and the combination of Candidate and Ground links are shown in Fig. 1 (b-n).

Triangles can be categorized as Equilateral, Isosceles, or Scalene based on the lengths of their sides. Depending on the side lengths and the possible assignment of the Candidate and Ground links, there are 13 ways to introduce a node in a triangle and transform it into a flat-foldable linkage. In our analysis, we assume that the side lengths of the triangles satisfy the inequality  $L_1 < L_2 < L_3$ . All sides have the same length for an *Equilateral* triangle, and any valid combination of the Candidate and Ground links results in the same configuration. As a result, there is only one way to introduce a node in an equilateral triangle—at the midpoint of the Candidate link. The formula to find length  $S$  in this case is illustrated in Fig. 1 (b).



**Fig. 1.** (a) Decomposing a triangle into a Grashof quadrilateral linkage, following the *flat-foldability* criterion; The location of the node to be introduced in a triangular is determined by calculating the length of the shortest link  $S$  when the triangle is: (b) Equilateral; (c - e) Isosceles with the common sides larger than the third side. (f - h) Isosceles with the common sides smaller than the third side; (i - n) Scalene. For all triangles,  $L_1 < L_2 < L_3$ . The Ground link is shown with a hatched side.

*Isosceles* triangles can be of two types. First, the sides of equal length are longer than the third, and second, the sides of equal length are shorter than the third. When the two equal sides of a triangle are longer than the third side, there are three possible orientations for the Candidate and Ground links: (Fig. 1c) the shorter side serves as the Ground link, and one of the longer sides is the Candidate link, (Fig. 1d) one of the longer sides serves as the Ground link, with the other longer side as the Candidate link; and (Fig. 1e) one of the longer sides serves as the Ground link, with the shorter side as the Candidate link. The formulae to find length  $S$  in these three cases when the sides equal in length are longer than the third side are shown in the respective figures. Similarly, when the two equal sides of a triangle are shorter than the third side, we have three more possible orientations for the Candidate and Ground links, as shown in Fig. 1 (f-h). The formulae to find length  $S$  in these three cases when the sides equal in length are shorter than the third are shown in respective figures. Thus, when we encounter an Isosceles triangle in a truss, there are six different ways to introduce a node.

In the case of a *Scalene* triangle, where all sides are unequal in length, there are six possible combinations of the Candidate and Ground links. For each of these six possible combinations, the formulae to determine the length  $S$  at which the node must be placed along the Candidate link are shown in Fig. 1 (i-n).

### 2.3. Workflow for system level node placement

In this subsection, we outline a workflow for identifying a Candidate link in each triangular unit of a static truss by considering both member forces and the configuration of adjacent triangles. We then apply the unit-level rules to introduce a new node on the Candidate links, enabling system-level reconfigurability for the initially static trusses.

Although any truss member within a triangular unit can be split by introducing a node, we focus on tensile members as Candidate links in our work. When subjected to loads, a node introduced on a tensile member remains stable without requiring locking or additional treatment. In contrast, splitting a compressive member requires locking the reconfigurable node in its deployed state to prevent unintended movement, which adds to the complexity of the deployment process. More-

over, introducing a node on a compressive member makes the structure vulnerable to buckling failure, as even minor imperfections that prevent the two links from being collinear would induce bending moments. Theoretically, limiting our focus to tensile members also preserves the structure’s stiffness and peak load capacity while enabling reconfigurability. Incorporating compressive members as Candidate links could provide alternative pathways for introducing reconfigurability into truss structures, which will be explored in future work. It is important to note that the distinction between tensile and compressive members is valid for a range of load cases that result in the same overall combination of tensile and compressive members in a given truss. Load cases outside of this range would require re-evaluation based on the new tensile and compressive member assignment.

With the selection criteria in place, we now detail a workflow that is programmed into an algorithm to identify and process Candidate links across an entire truss structure. We work with the following simplifying assumptions. First, we assume the trusses are planar. Second, we restrict the scope of the workflow to trusses composed of a single layer of triangular units arranged in sequence between the top and bottom chords. Third, we assume the truss is statically determinate. Based on these assumptions, the workflow processes each triangle sequentially, tracking the following elements within the truss at any given step: (i) Ground link,  $G$ ; (ii) Candidate link,  $C$  (not to be confused with compressive link); (iii) Avoid link,  $A$ ; (iv) Current triangle,  $\Delta_c$ ; (v) Previous triangle,  $\Delta_p$ ; and (vi) Next triangle,  $\Delta_n$ . At each step within the current triangle, the Ground link ( $G$ ) is typically defined as the side shared with the previous triangle ( $\Delta_p$ ), while the Avoid link ( $A$ ) refers to the side shared with the next triangle ( $\Delta_n$ ).

To demonstrate how the Candidate link is selected, let us consider the cantilever truss example in Fig. 2. In Step 1, the triangles are numbered, and the tensile and compressive members are identified. Starting from Step 2, each triangle is analyzed individually. To start in Step 2,  $\Delta_1$  is the current triangle and  $\Delta_2$  is the next. The member between the two supports acts as the Ground link, while the side shared between  $\Delta_c$  and  $\Delta_n$  becomes the Avoid link. The remaining side, being a tensile member, is designated as the Candidate link ( $C$ ), and a node is introduced based on the rules described in Section 2.2, which consider the lengths of  $G$ ,  $C$ , and  $A$ .

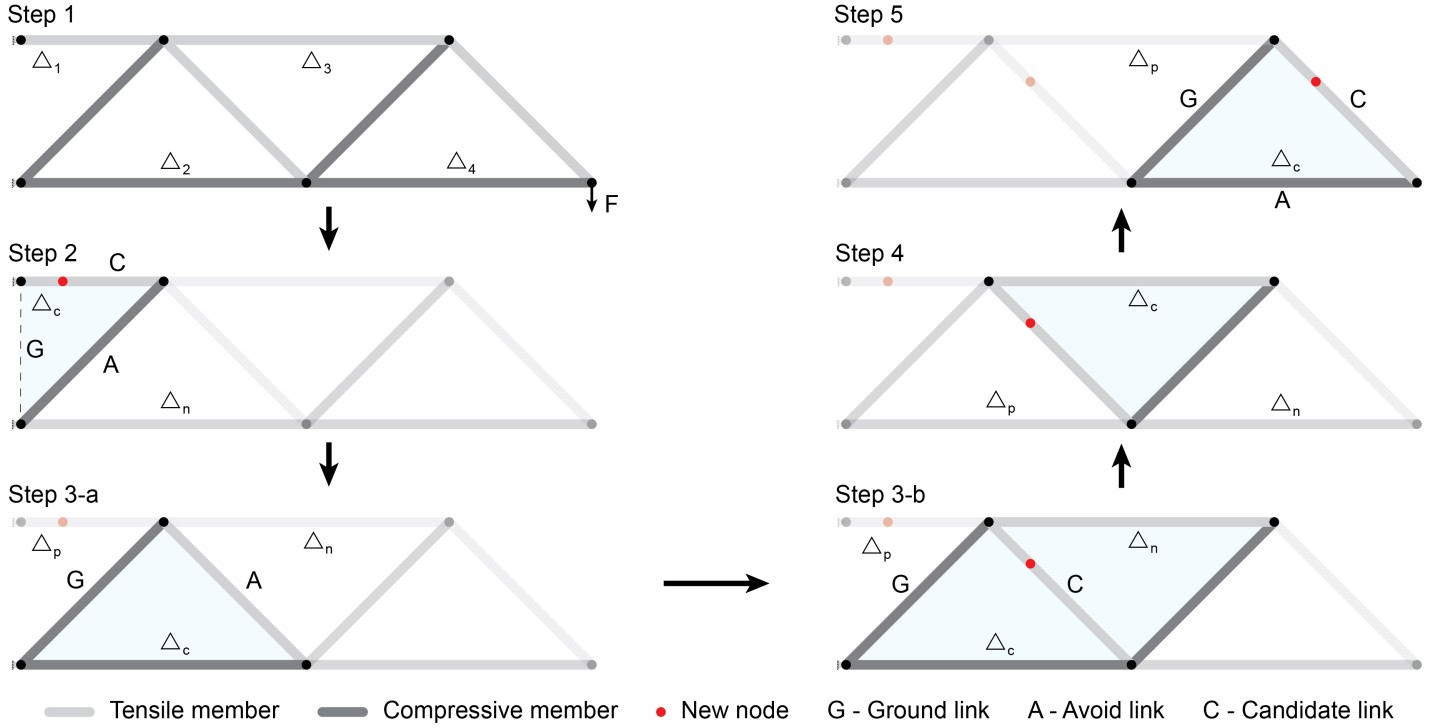


**Fig. 2.** A visual representation of how the workflow processes triangles sequentially to introduce nodes.

In Step 3-a,  $\Delta_2$  becomes the current triangle, with  $\Delta_1$  and  $\Delta_3$  as the previous and next triangles, respectively. The Ground and Avoid links are assigned as described earlier. Because the third side of  $\Delta_c$  is not a tensile member, we check whether the Avoid link is tensile and if  $\Delta_c$  and  $\Delta_n$  are congruent. If both conditions are satisfied, the avoid link is reclassified as the Candidate link, and a node is introduced based on the side lengths of the current triangle, as shown in Step 3-b. This approach consolidates two triangular units into a unique 6-bar linkage with a single kinematic degree of freedom. If the two triangles are not congruent, the same operation could be performed, however the system would not be able to fold flat.

The process continues to Step 4, where  $\Delta_3$  becomes the current triangle. Throughout the process, we maintain a history of the nodes introduced in the structure. If a node has already been placed on the Ground link of the current triangle in the previous step, the workflow skips that triangle to avoid placing multiple nodes in a triangle. Consequently, in Step 4, no new node is added, and we proceed to the final triangle. This approach ensures that only one new node is introduced for any given triangle.

In Step 5,  $\Delta_4$  becomes the current triangle, with  $\Delta_3$  as the previous triangle. The common side between the two triangles is assigned as the Ground link. Of the two remaining sides, the compressive member becomes the avoid link while the tensile member is assigned as the candidate link. A node is then introduced on this Candidate link.

While this process applies to most triangles in the truss, three additional rules are embedded in the workflow to handle special cases. First, if the first triangle in the structure does not have two support nodes, the compressive member connected to the support node is classified as the Ground link. Second, the workflow skips the current triangle, leaving it as a static part of the system if: (a) none of the non-ground links are tensile, or (b) the side shared between  $\Delta_c$  and  $\Delta_n$  is tensile but the triangles are not congruent. Therefore, only the tensile nature of the non-ground links is considered for the selection of the Candidate link. Third, the tensile member with the higher cross-sectional area is selected as the Candidate link if two tensile members exist in the current triangle and no side is shared with the next triangle. A video illustrating the steps of the proposed workflow is provided as Supplementary Video 1.

Each node (pinned joint) introduced by the proposed workflow introduces a degree of freedom, imparting a mobility of one to the truss system. This added mobility, while enabling the structure's reconfigurability, introduces potential movement that renders the system structurally unstable. However, upon the application of an external force, tensile forces are generated along the members where new nodes have been introduced. This tension effectively secures the pinned joints, as the force pulls the tensile members taut, limiting relative movement around each pin. Consequently, the applied force stabilizes the structure under load. Thus, the reconfigurable trusses generated through our approach can be considered force-stable and can exhibit shape-morphing behavior in the absence of an applied external load.

### 3. Transforming traditional trusses into reconfigurable systems

In this section, we demonstrate the reconfigurable trusses obtained with the proposed method and examine their spatial movement using three representative designs commonly found in prac-

tice: (i) Scissor truss, (ii) Fink truss, and (iii) Warren truss.

A sequential kinematic simulator was developed to analyze the kinematic behavior of the modified truss systems. This program utilizes the analytical solution of a planar quadrilateral linkage to simulate the motion of each kinematic degree of freedom (DOF) in the structure, one at a time. Users can specify the extent of actuation for each DOF, with 0% representing the initial state and 100% corresponding to the flat-folded configuration. At 0% actuation, the decomposed links of the Candidate link are collinear, forming an angle of 180° relative to each other. An X% actuation corresponds to X% of the total angular rotation required to rotate the shorter of the decomposed links relative to the Ground link and make them collinear. Depending on the geometry of the quadrilateral linkage, the 100% actuated state results in the shorter of the decomposed links folding to either 0° or 180° relative to the Ground link. Details are provided in A.3.

During the actuation of each DOF, we track two parameters to assess the packing density of the structure as it changes shape. The packing density is evaluated using: (i) area of the convex hull,  $\text{Conv}(\cdot)$  of the truss nodes, and (ii) the maximum length of the truss structure. The convex hull of a set of points in a plane (or in higher-dimensional space) is the smallest convex shape that contains all the points in that set (Tyrrell Rockafellar, 1970). As the truss morphs, the convex hull area is normalized by its initial, non-actuated area to measure relative compactness. The maximum length of the truss is defined as the greatest distance between any two points within this convex hull and is normalized by the initial maximum length of the truss to provide a consistent basis for comparison across configurations.

Figure 3 (a) demonstrates the step-by-step actuation of each kinematic degree of freedom in a Scissor truss, which has been modified using our proposed method to enable reconfigurability. Five new nodes (highlighted in red and numbered) have been introduced, resulting in five independent kinematic DOFs numbered from one to five from left to right. Moving sequentially from left to right in Fig. 3 (a), each DOF is actuated up to 85% of its maximum limit (approaching a flat state). While each DOF could theoretically reach 100%, we limit the actuation to 85% here to provide a more clear visualization of the kinematic motions. Throughout this actuation process, the area of the convex hull (left axis) and the maximum length of the hull (right axis), are tracked and

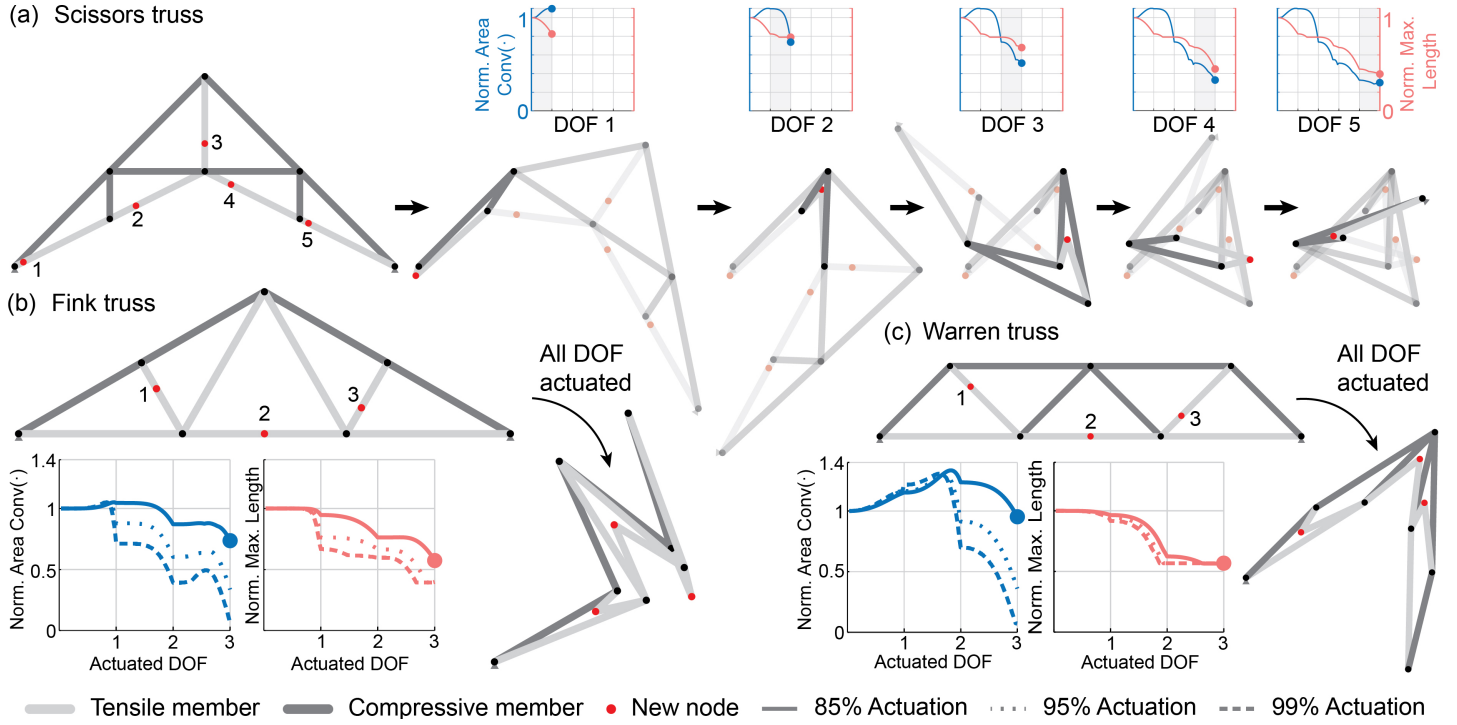


**Fig. 3.** (a) Sequential actuation of each kinematic degree of freedom, illustrating the kinematic path of a reconfigurable Scissor truss. The dual Y-axis plot displays changes in the convex hull area normalized by the initial convex hull area of the truss (left axis) and the maximum structural length normalized by the initial maximum length of the truss (right axis) as the configuration evolves. The initial and final configurations after actuating all kinematic degrees of freedom are shown for (b) the Fink truss and (c) the Warren truss, along with the normalized convex hull area and maximum length plots for 85%, 95%, and 99% actuation of each DOF.

illustrated in the plots above each actuated DOF in Fig. 3 (a). Even with each DOF actuated only to 85%, the structure achieves a compacted area that is approximately 0.3 times its initial footprint. The structure also achieves a reduction in maximum length to about 0.4 times the initial truss length when all DOFs are actuated to 85%.

Figure 3 (b) and (c) illustrate the Fink and Warren trusses in their pre-actuation and post-actuation states, respectively. The post-actuation configurations illustrated here are achieved by actuating each kinematic DOF to 85% of its initial state for each truss. For both trusses, we also demonstrate the changes in the structure’s convex hull area and the maximum length compared to their initial states. These changes are depicted for three cases, wherein each DOF is actuated to 85% (solid), 95% (dotted), and 99% (dashed) of its initial state.

For the Fink truss, we observe that actuation of 85%, 95%, and 99% across all three DOFs results in the compacted structure achieving a convex hull area of 0.73, 0.34, and 0.07 times its initial state, respectively. Correspondingly, the maximum length of the compacted structure is reduced to 0.57, 0.39, and 0.39 times the initial length. In the case of the Warren truss, actuation of 85%, 95%, and 99% across all three DOFs reduces the compacted structure’s convex hull area to 0.95, 0.36, and 0.07 times its initial state, respectively. The reduction in the maximum length of the structure plateaus at 0.56 times its initial state, irrespective of the extent of actuation of each kinematic DOF of the truss.

From the three examples of reconfigurable trusses, we observe varying levels of compactness based on the type of truss and the extent of actuation. For instance, the scissor truss achieves significant reduction of the convex hull area even with 85% actuation of its DOFs (final state that is  $0.3\times$  of the initial). In contrast, the Fink and Warren trusses show a minimal reduction in their footprint at the same actuation (final states that are  $0.7\times$  and  $0.9\times$  of their initial). However, with 99% actuation of all DOFs, all three trusses achieve up to a 93% reduction in convex hull area. In other words, if we can sufficiently actuate all the DOFs of the system, we can achieve a large reduction in the overall area that a stowed truss will take up. It is important to note that this level of compact packing is theoretical and can only be achieved if the overlap of structural members is allowed. In practical applications, strategies like distributing bars in and out of the

plane (as discussed in Section 5.1) must be implemented to achieve adequate packing without overlap. Furthermore, while a large reduction in the volume of the truss is possible, the maximum length of the truss can be reduced to only a fraction of the initial length, such as  $0.4\times$  for the Scissor,  $0.4\times$  for the Fink, and  $0.5\times$  for the Warren truss. Often the reduction in maximum length of the truss plateaus with the first DOFs, and further actuation of the system does not produce a notable reduction in the system length. For instance, when actuating the Warren truss, the compressive members on the side and the top chord of the truss become collinear, and do not fold further, even as the system becomes flat.

## 4. Reconfigurable trusses for arbitrary geometries

In this section, we show that our approach enables the transformation of arbitrary truss geometries into reconfigurable systems. We apply our node introduction workflow to trusses obtained using topology optimization for arbitrary geometries, loads, and support conditions. We first discuss how our method can be integrated with ground-structure-based topology optimization and then discuss how results from continuum optimization can be adopted into reconfigurable systems.

### 4.1. Arbitrary truss geometries from ground-structure-based topology optimization

In this subsection, planar trusses for arbitrary geometries, loads, and support conditions are obtained using the ground-structure-based topology optimization method (GRAND) developed by Zegard and Paulino (2014). GRAND begins by discretizing the design domain into a mesh of nodes connected with a network of potential truss members to form the *ground structure*. The complexity of the network is determined by a parameter called connectivity level. At level 1 connectivity, each node is connected only to its immediate neighbors, resulting in a sparse network. Higher connectivity levels introduce connections to distant nodes, adding potential members and redundancy to the structure. Selecting an appropriate connectivity level is crucial, as it influences the complexity of the resulting design and computational effort.

The goal of the optimization is to identify the lightest truss structure that satisfies the given

load and support conditions. GRAND achieves this goal by minimizing the total volume of material of the truss members,  $V = l^T a$ , where  $l$  and  $a$  represent the lengths and cross-sectional areas of the members, respectively. The method redistributes material among truss members by adjusting their cross-sectional areas and removing unnecessary members whose areas fall below a user-defined threshold. The optimization process maintains static equilibrium and keeps member stresses within allowable limits to ensure the final design meets all structural performance criteria while minimizing material use.

Truss structures generated using GRAND require post-processing before being integrated with our node introduction workflow to create reconfigurable trusses for arbitrary geometries. Since GRAND often outputs trusses with unused nodes and bars with zero cross-sectional area, the first step involves removing unused elements, renumbering the nodes, and updating the bar connectivity. The next step identifies nodes connected to exactly two collinear bars. These nodes are removed, and the collinear bars are replaced with a single bar whose cross-sectional area is the maximum of the two original bars. The optimized structure may also lack a direct connection between the support nodes due to the specified boundary conditions. This lack of connection is addressed by introducing zero-force members between the supports with a cross-sectional area equal to the minimum of the bar areas in the optimized structure. Additionally, if intermediate nodes lie along the line connecting the supports, zero-force members are added to connect all collinear nodes. Occasionally, a stray bar may connect the force application point to the rest of the structure. In such cases, the node of force application is connected to the nearest available node on the structure or directly to a support. These post-processing steps ensure that the resulting truss structure is primarily composed of closed triangular units.

As an illustrative example, Fig. 4(a, top left) shows a level-1 ground structure loaded as a cantilever. This structure is first optimized using GRAND and then post-processed and transformed into a reconfigurable system using the proposed method of node introduction. Sequential kinematic simulations are performed on the reconfigurable cantilever truss to examine its kinematic behavior in space. The reconfigurable cantilever truss exhibits a reduction in the convex hull area up to 0.34, 0.12, and 0.07 times its initial state when all three kinematic DOFs are actuated to 85%, 95%, and 99%, respectively. In contrast, the reduction in the maximum length of the structure is minimal

and plateaus at 0.97 times its initial length despite the full actuation of all DOFs.

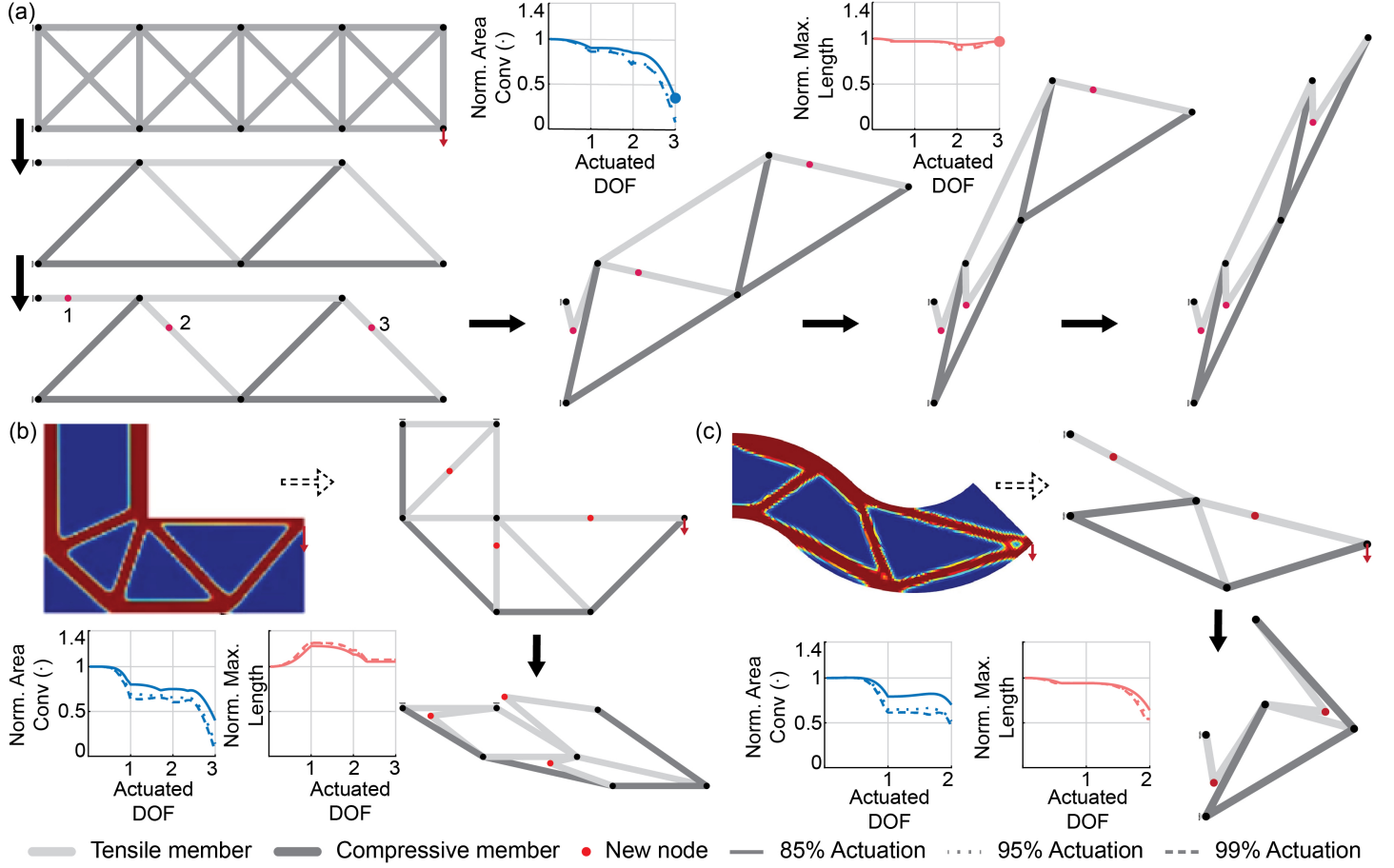


**Fig. 4.** (a) Cantilever truss. Anti-clockwise from top left: level-1 ground structure for a cantilever problem, optimized cantilever truss obtained from ground structure optimization, cantilever truss transformed into a reconfigurable structure, and sequential actuation of each kinematic degree of freedom up to 85% of its full extent. Plots depicting the convex hull area and maximum length of the structure, relative to its initial state, are shown for 85%, 95%, and 99% actuation of each DOF of the structure morphs; (b) L-shaped and (c) Serpentine truss. Clockwise from top left: topology optimized structure (adapted from Ullah et al. (2022) under the Creative Commons Attribution 4.0 International License), approximate simplified truss structure modified to obtain a reconfigurable system, stowed orientation of the structure at 85% actuation of all DOFs, variation in normalized maximum length and normalized convex hull area of the structure at 85%, 95% and 99% actuation of all DOFs.

While the topology-optimized cantilever truss effectively demonstrates the applicability of the proposed method for trusses with arbitrary geometries, the transformation process becomes increasingly challenging as the domain shapes become complex. For instance, consider the L-shaped

and Serpentine beams illustrated in Fig. 4(b) and (c), respectively. The ground-structure-based topology optimization of these geometries can exhibit highly intricate bar connectivity, including overlapping bars and polygonal shapes. Currently, our workflow is not equipped to handle such complex structures — a limitation we identify as a key direction for future work (see Section 6.2).

#### *4.2. Arbitrary truss geometries from continuum topology optimization*

Continuum topology optimization has become a widely adopted tool in structural engineering for identifying the efficient distribution of material within prescribed design constraints. While similar to ground-structure optimization, continuum optimization does not enforce strict stress constraints during the optimization process. Instead, the continuum optimization works by optimizing the stiffness or compliance by adjusting the distribution density of continuous material in a domain. Various continuum optimization methods have been developed that serve as conceptual guides for engineers designing new structures (Sigmund and Maute, 2013). However, raw results from continuum optimization often require additional filtering or post-processing to ensure structures have fewer, well-defined and practically manufacturable members, particularly in civil engineering applications where direct additive manufacturing is impractical. Engineers frequently use their judgement to simplify intricate continuum optimization results into simpler truss-like designs that retain core load-carrying mechanisms while accommodating design constraints such as domain geometry, loads, and supports (Zegard et al., 2020). In line with this practice, we use simplified versions of continuum-optimized structures as the starting point for our reconfigurable truss designs.

We use the continuum-optimized results from Ullah et al. (2022) (adapted under the Creative Commons Attribution 4.0 International License) as a benchmark for the L-shaped truss and serpentine truss designs. The simplified versions of these trusses, which can be transformed into reconfigurable systems, are presented in Figures 4(b) and (c), respectively. These examples are chosen from the literature for simplicity, though other continuum-optimized structures could also be adapted using the same approach. We intentionally select slender geometries that resemble single-chord truss systems and make geometric modifications to ensure compatibility with our

node introduction workflow. In cases where a quadrilateral is encountered in the continuum-optimized structures, we either add a diagonal to split it into two triangles or remove the shortest member to reduce it to a single triangle. For the L-shaped domain, the geometry is adjusted to obtain congruent triangles. While these simplified structures differ from the original continuum-optimized designs, they still fit within the initial envelope and carry a load using the same overall mechanisms. The morphed configurations of these two truss structures at 85% actuation of each degree of freedom are shown in Fig. 4 (b) and (c).

We observe that the L-shape truss, when actuated to 85%, 95%, and 99% across all three DOFs, reduces its convex hull area to 0.4, 0.14, and 0.06 times its initial state, respectively. Correspondingly, the maximum length of the compacted structure increases to 1.05, 1.07, and 1.07 times the initial length. While the L-shaped truss effectively reduces the area it occupies, the increase in maximum length (about 7%) occurs because the structure flattens along its longest side in the final state. For the Serpentine truss, one triangular unit remains unaffected by the node introduction workflow due to the compressive nature of the bars and the non-congruent next triangle (a constraint established earlier in this paper). Nonetheless, an actuation of 85%, 95%, and 99% across all two DOFs of the Serpentine truss reduces the convex hull area to 0.7, 0.52, and 0.45 times its initial state, respectively. The maximum length of the compacted structure was reduced to 0.64, 0.54, and 0.54 times the initial maximum length of the truss, respectively. We acknowledge the challenges of rendering these complex truss structures reconfigurable and have identified them as potential areas for future research.

## 5. Physical design of reconfigurable trusses and proof-of-concept prototypes

This section outlines the basic design principles, physical fabrication, and mechanical performance of the reconfigurable truss systems introduced in this paper. First, we introduce the strategies used to distribute truss members in and out of the plane, ensuring proper shape-morphing behavior while avoiding out-of-plane bending moments during loading. We then detail the fabrication of two reconfigurable truss structures — a cantilever truss and a Warren truss, and load test these structures to demonstrate that these systems maintain stiffness and strength, making them

suitable for large-scale applications.

### *5.1. Distributing truss members in and out of plane*

Real-world static planar trusses typically consist of members that converge at the nodes or joints along the central plane of the truss. This member placement ensures load transfer along the central plane of the truss without generating out-of-plane bending moments that could induce global deformations and buckling. However, placing members in the same plane at every joint is incompatible with the reconfigurable truss designs presented in this study. Our designs must account for member contact and avoid overlap to ensure the expected shape-morphing behavior. The reconfigurable trusses must, therefore, be fabricated using techniques that strategically distribute truss members across the central plane to ensure desired shape transformations and a densely packed state. This distribution of members must ensure that the applied loads are distributed evenly about the central plane without generating unwanted out-of-plane bending moments.

We utilize a color-coded schematic to illustrate the distribution strategy of truss members across the central plane. This schematic assigns a specific color to each truss member based on its distance from the central plane, organizing them into distinct levels, as illustrated in Fig. 5 (a). Members marked in red are placed closest to and immediately on either side of the central plane. Green-marked members are placed at a distance of one member thickness, blue at two, yellow at three, and purple at four member thicknesses. The proof-of-concept prototypes are fabricated with a two-ply configuration incorporating the color-coded schematic to define the separation between member levels. Each truss member in the two-dimensional trusses shown in Fig. 5 (b) and (e) has a corresponding member positioned equidistantly on the opposite side of the central plane. This two-ply configuration ensures that loads act along the central plane, preventing moment generation that could induce torsional deformations in the structure.

To ensure the truss exhibits the expected shape-morphing behavior and achieves a compact folded state, we aim to nest members as close to the central plane as possible. This arrangement is illustrated for select joints in the fabrication of the reconfigurable cantilever and Warren trusses in Fig. 5 (c) and (g), respectively. Nesting the morphing members in this manner allows them to

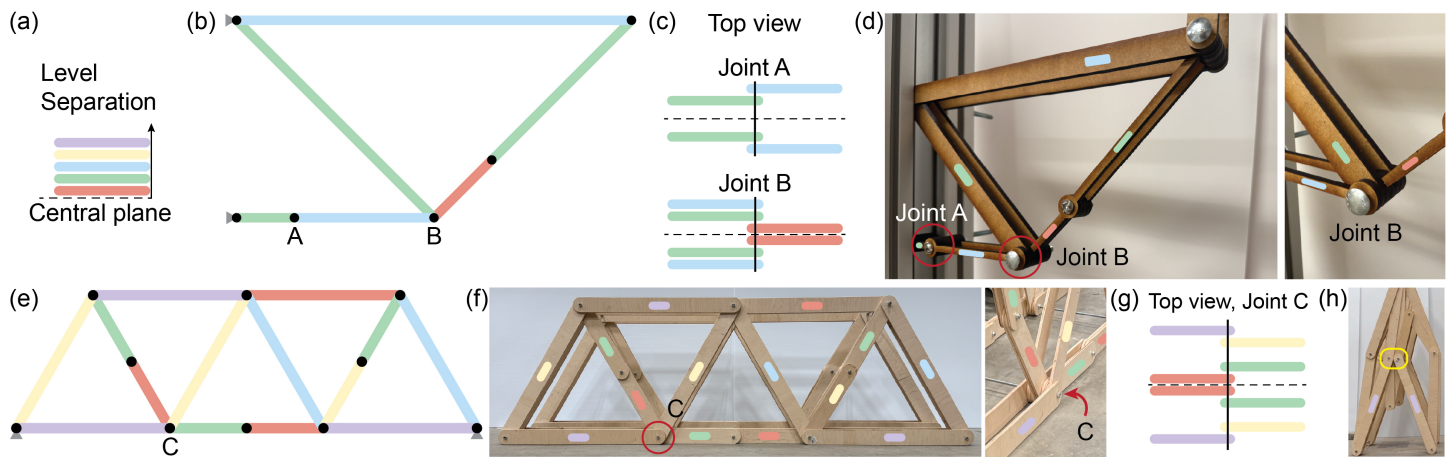


**Fig. 5.** (a) Color-coded schematic of the out-of-plane level separation of truss members; (b) Side view of reconfigurable cantilever truss indicating the out-of-plane level separation of its members; (c) Top view of joints A and B illustrating the position of the members across the central plane (dashed); (d) Oblique view of the reconfigurable cantilever truss prototype showing the fabricated joints A and B; (e) Side view of reconfigurable Warren truss indicating out-of-plane level separation of its members; (f) Side view (left) and oblique view of joint C (right) of the fabricated reconfigurable Warren truss prototype indicating out-of-plane level separation of its members; (g) Top view of joint C illustrating the position of the members across the central plane (dashed); (h) Truss members coded with the same color cannot overlap and thus would encounter contact as the structure is folded towards a compact state (highlighted by the lilac ellipse).

achieve a dense folded state while keeping the unit self-contained and preventing member contact. Since the prototypes follow a two-ply configuration, the width of each joint becomes at least twice the sum of the widths of all connected members in the two-dimensional design. As the complexity of the structure increases, particularly when more members converge at a single joint, members need to be positioned farther away from the central plane. In such cases, achieving the desired shape transformation may require more layers than simply twice the number of members connected to the joint in the two-dimensional design. An example of this case is depicted in Fig. 5 (g), where four members meet at joint C, yet the joint's width exceeds twice the sum of the widths of all connected members. This additional width is necessary when considering the entire design of the truss system in Fig. 5 (e).

An important observation is that increasing the number of layers alone may not be enough. Proper nesting of joint components is also crucial. Protruding joint edges can prevent the system from folding all the way and lead to an inefficiently packed structure, even with adequate layer spacing at individual joints. For example, the Warren truss cannot fold completely flat because members with the same separation level encounter contact as the structure folds towards a compact state (Fig. 5 h). Optimizing for compactness requires careful joint design, either by nesting protruding edges within member bodies or by ensuring joints lay flush with member surfaces. Proper nesting will help achieve a more efficient folded state. Future work can refine these design strategies to improve structural compactness and reconfigurability.

## *5.2. Comparison of stiffness and strength between reconfigurable and static trusses*

The static and reconfigurable versions of a cantilever truss, shown in Fig. 6 (b) (left and right, respectively), were fabricated using the strategies discussed in Section 5.1. Each truss member was laser cut out of a 6.35 mm thick Medium Density Fiberboard (MDF) sheet. Consequently, all members had a cross-sectional width of 6.35 mm when viewed from the top, as illustrated in Fig. 6(a, top). The tensile members featured a square cross-section of 6.35 mm by 6.35 mm, with side profile dimensions as depicted in Fig. 6(a, bottom). The compressive members had a rectangular cross-section, measuring 6.35 mm in width and 19.05 mm in depth, with side profile

dimensions as shown in Fig. 6 (a, middle). The increased depth of the compressive members was chosen to prevent buckling and ensure structural failure by fracturing the tensile members. Truss components were assembled using 6.35 mm bolts, with connections designed to allow rotational movement rather than friction-based locking. Both truss configurations were tested under a loading rate of 12.7 mm/min using the Mark-10 ESM1500 load testing machine. The trusses were mounted on a test frame with pinned connections using 6.35 mm bolts. The test frame was constructed from 80-20 aluminum extrusions and firmly secured to the Mark-10 machine with machine screws. Displacements of the test frame observed during sample testing were orders of magnitude smaller than those experienced by the tested trusses. Therefore, the frame can be reasonably assumed to act as a rigid body for connecting the trusses.

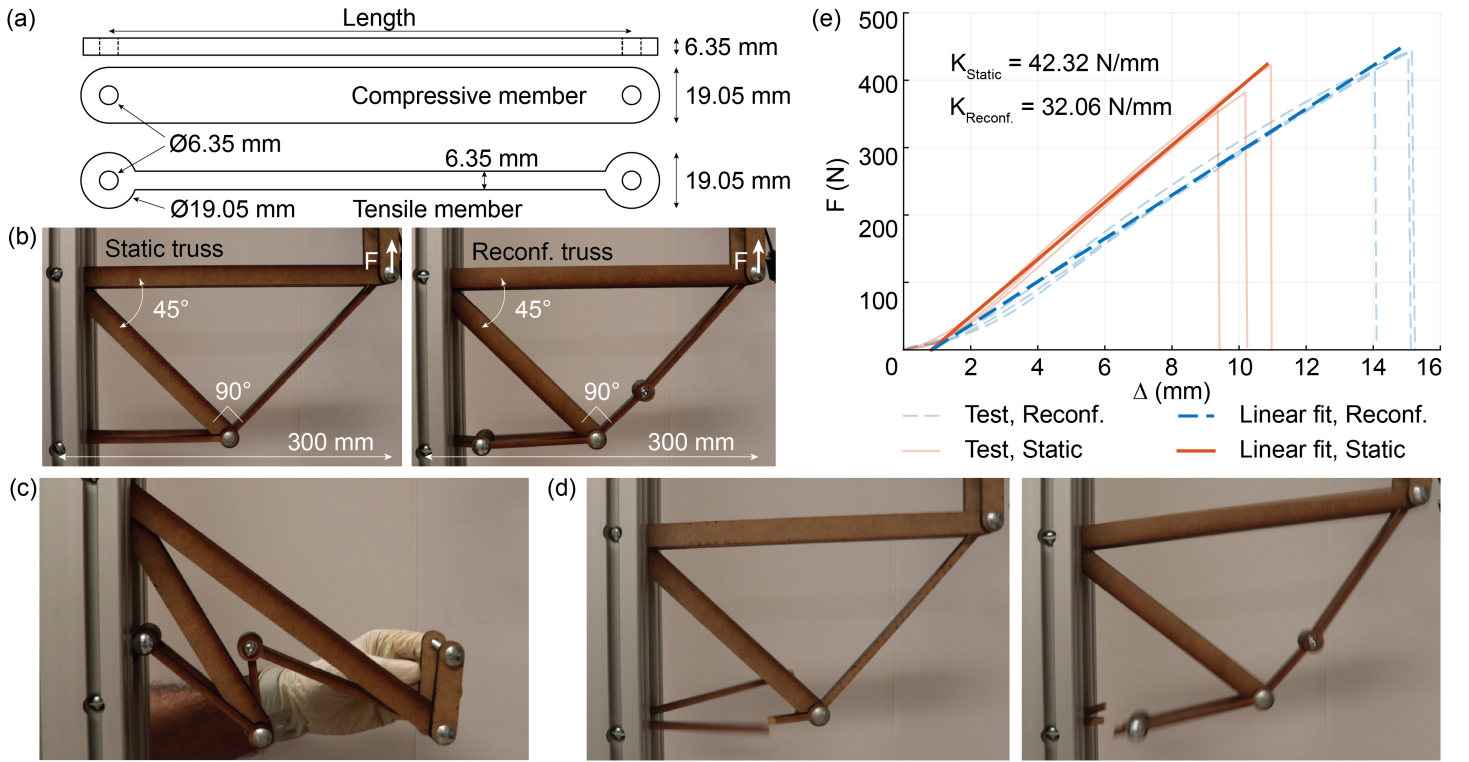


**Fig. 6.** (a) Dimensions of the members used for the cantilever truss: top view of all members (top), side view of the compressive (middle) and tensile (bottom) members; (b) Static (left) and reconfigurable (right) versions of the cantilever truss on Mark-10 ESM1500 testing rig; (c) Stowed configuration of the reconfigurable cantilever truss; (d) Failure of the tensile members of the static (left) and reconfigurable (right) cantilever truss; (e) Load-displacement curves for the static and reconfigurable cantilever truss. Faint lines depict the raw data from three separate load tests, while the opaque lines represent the fitted curves used to calculate the stiffness.

Three samples of each truss configuration—static and reconfigurable—were load tested to compare structural performance. Both configurations exhibited failure through tensile fracture of the bottom member as depicted in Fig. 6 (d). The static trusses exhibited an average peak load capacity of 387 N and a stiffness of 42.32 N/mm, while the reconfigurable truss exhibited an average peak load capacity of 433 N and a stiffness of 32.06 N/mm. The theoretical peak load for the two-ply truss design was calculated as 725 N, with a displacement of approximately 3 mm at the loading point, resulting in a calculated stiffness of 241 N/mm. The yield forces for individual members were determined as 725 N for tensile and 806 N for compressive members. Additionally, the critical buckling load for the longest compressive member was calculated to be 982 N, ensuring that failure does not occur due to member buckling. These theoretical values were derived using a Young’s modulus ( $E$ ) of 4 GPa, tensile yield stress ( $\sigma_{Ty}$ ) of 18 MPa, and compressive yield stress ( $\sigma_{Cy}$ ) of 10 MPa based on Ross et al. (2010). A video of the load tests for both the static and reconfigurable cantilever trusses is included in Supplementary Video 2.

Two key discrepancies were observed in the test results. First, the static and reconfigurable trusses showed differing peak load and stiffness despite their expected equivalence. Second, the experimental peak load and stiffness were significantly lower than theoretical predictions. The lower stiffness of the reconfigurable truss can be attributed to increased joint slip due to the higher number of joints present compared to the static truss. This slipping delays the full engagement of the members and is evident from the higher displacement of the loading point in the load-displacement curves of the reconfigurable truss (indicated by faint blue dashed lines in Fig. 6 (e)). The reconfigurable truss also contains more material than the static truss. Because the structure is tested by pulling upward, this additional material requires a greater force to overcome the increased gravitational resistance before reaching the failure load in the members. As a result, the reconfigurable truss exhibits a higher peak load than the static truss.

The difference between experimental and theoretical performance likely stems from a combination of (*a*) weakening of the mechanical properties of MDF due to the degradation of its internal structure caused by extreme heat applied during laser cutting (Lum et al., 2000; Mushtaq et al., 2020); and (*b*) joint play caused by non-zero clearance between the screw and the hole. Each joint in the truss assembly is far from ideal and exhibits play, which increases structural displacements

under loading. This non-ideal joint behavior further contributes to the observed reduction in stiffness compared to theoretical values. We also believe the joint interplay reduces the strength of the system because parallel members, while equidistant from the central plane, may still carry unequal forces, causing one member to fail first. The combined effects of material degradation and joint play are also reflected in the fluctuating peak loads observed across individual tests, providing additional insight into the deviations in peak load capacity between the two trusses.

Despite the observed discrepancies, the static and reconfigurable trusses exhibit reasonably high peak load and structural stiffness that are close to each other. With the improved fabrication of joints and members, we expect the trusses to reach strength and stiffness comparable to the theoretically predicted values.

### *5.3. Structural behavior of a three meter long reconfigurable Warren truss bridge*

A three-meter-long reconfigurable Warren truss bridge, shown in Fig. 7 (b), was fabricated to demonstrate the scalability of the proposed method for large-scale reconfigurable trusses. The truss members were cut from 1.27 cm thick Maple plywood sheets, giving them a cross-sectional width of 1.27 cm, as seen in the top view in Fig. 7 (a, top). Each member had a 1.27 cm diameter hole at both ends and a cross-sectional depth of 10 cm, as shown in the side view in Fig. 7 (a, bottom). The Warren truss featured members of two lengths: 1 m and 0.5 m (center-to-center between joint holes). Member connections were made using 1.27 cm diameter steel threaded rods secured with machine screw nuts. These joints were designed to allow member rotation without acting as a friction joint, enabling the truss to be reconfigured and stowed compactly, as shown in Fig. 7 (c) and Supplementary Video 2. The truss also featured a two-ply configuration to ensure that loads were transferred along the central plane of the truss without inducing moments. Two identical Warren trusses were assembled with an out-of-plane offset, as shown in Fig. 7 (b, right), resulting in a total structural width of 0.6 m. The truss was laterally braced with 0.16 cm steel cables to prevent global buckling.

Next, a three-point load test was conducted using an Instron machine to evaluate the structural behavior of the reconfigurable Warren truss bridge. The truss was simply supported at the

end nodes, with the load applied at the center across its entire width. Figure 7(d) illustrates the schematics of the loading point and support constraints. Loads were applied cyclically in a displacement-controlled manner, with the structure subjected to two loading cycles at each specified displacement, except for the first and last displacements. The applied displacements were 3.6 mm, 7.1 mm, 7.6 mm, 8.6 mm, 10.2 mm, 12.7 mm, 15.3 mm, 17.8 mm, and 20 mm. The load-displacement response of the cyclic three-point load test is presented in Fig. 7(e). The load-displacement curve revealed slight structural degradation between the first and second cycles for every specified displacement, with the peak load being lower by an average of 2.4% in the second cycle. However, there was an average increase of 17% in stiffness during the second cycle compared to the first at the same displacement level. By the final loading stage, the structure had accumulated approximately 7 mm of downward plastic deformation. The loading phase of the first cycle at each specified displacement was plotted against the displacement of the structure after removing accumulated residual deformation to explore stiffness degradation during loading. The resulting load-displacement curve is presented in Fig. 7(f). The truss exhibits initial stiffening after loading up to the first and second specified displacements due to the complete engagement of the joints and members. As shown in Fig. 7(g), the compressive members at the end of the structure exhibit some elastic buckling at loads as low as 50% of the failure load ( $F_p$ ). However, this buckling does not seem to impact the stiffness and load-displacement behavior of the structure. In subsequent loading phases, stiffness degradation occurs towards the end of each phase, with the most significant degradation observed in the final cycle. This degradation can be attributed to the relaxation of lateral bracing steel cables, marked by dips in the load-displacement curves in Fig. 7(e). The loss of cable tension results in insufficient bracing, leading to larger local buckling of truss members. This local buckling triggers global buckling as the load approaches the failure threshold, ultimately resulting in a critical local buckling with structural failure as depicted in Fig. 7(g).

The theoretical peak tensile and compressive forces for individual Warren truss members were determined as 4.726 kN and 4.286 kN, respectively, based on Maplewood's tensile yield stress ( $\sigma_{T_y}$ ) of 4 MPa and the compressive yield stress ( $\sigma_{C_y}$ ) of 3.6 MPa. For the given loading condition, a 1 kN load generated a maximum tensile and compressive force of 0.87 kN and 0.58 kN,

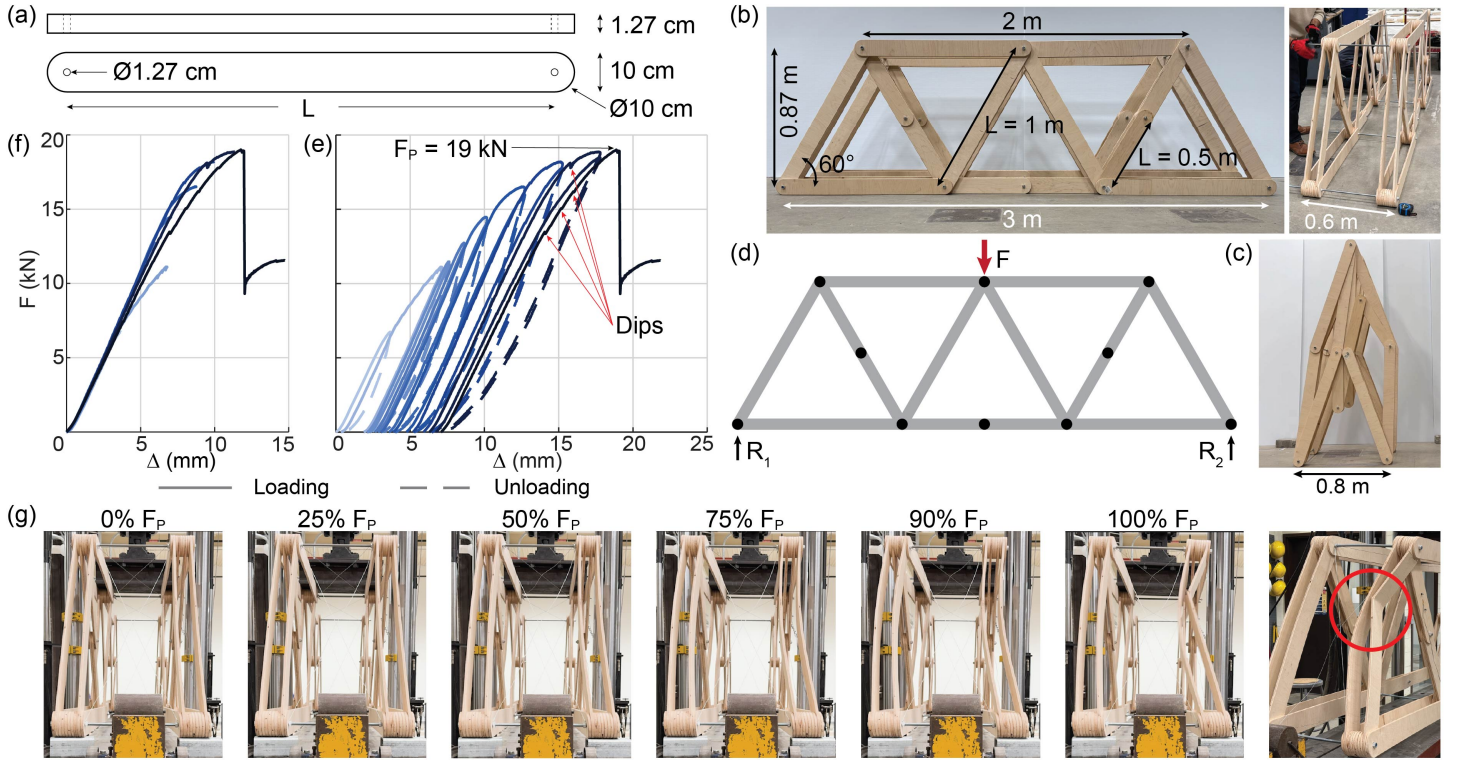


**Fig. 7.** Warren truss prototype. (a) Dimensions of the Maplewood members, shown in top (upper) and side (lower) views; (b) Side (left) and oblique (right) views detailing the overall dimensions of the structure; (c) Stowed configuration of the Warren truss bridge; (d) Schematic representation of the three-point-loading test, illustrating the load and supports; (e) Complete Load ( $F$ ) vs. Displacement ( $\Delta$ ) curve of the cyclic three-point-loading test. The truss weighs 38 kg and can support a load of 19 kN; (f) Load-Displacement curve depicting the initial loading phase of each cycle for all specified displacement limits after removing accumulated structural displacement; (g) End-view of the structure during loading—local elastic buckling of the truss members results in shortening of diagonals, which subsequently leads to larger global and local buckling as the structure approaches the point of failure.

respectively, in the members of a two-dimensional Warren truss. Since the Warren truss bridge prototype featured a four-ply configuration, its theoretical peak load capacity was calculated as 21.9 kN ( $4 \times 4.726/0.87$ ). At this peak load, the maximum compressive force in any member would be 3.13 kN ( $21.9 \times 0.58/4$ ), which is well below the yield compressive force and the estimated 4.52 kN critical buckling load for a 1 m long member, pinned at both ends. These calculations indicate that buckling should not have been the failure mode. During testing, however, the truss failed due to elastic buckling at a peak load of 19 kN, when the compressive force in the failed member was only 2.76 kN (much lower than all calculated limits). The observed buckling, contrary to the expected tensile failure, can be explained by the following three reasons. First, significant play in the truss connections introduced flexibility and caused unintended lateral movements during loading. Second, steel cables added to brace the structure against lateral movements were not tensioned uniformly. This non-uniform tensioning resulted in insufficient bracing and lateral-torsional buckling of the structure. Lastly, the inherent curvature of plywood members reduced their load capacity and made them susceptible to buckling. Additionally, dry weather conditions during the two-month gap between fabrication and testing likely caused the plywood members to lose moisture and increase their curvature. These reasons explain why we observe the initial elastic buckling of the system and the ultimate failure from buckling rather than the tensile fracture that was initially expected.

Despite fabrication defects and unexpected buckling failure, the reconfigurable Warren truss bridge (weighing 38 kg) sustained cyclic loading until failure at a peak load of 19 kN. The sustained load was just 13.2% lower than the theoretical peak load of 21.9 kN for the four-ply Warren truss. Future refinements in design and fabrication are expected to reduce this gap in load capacity. A video of the load test and failure of the Warren truss bridge is included in Supplementary Video 2.

## 6. Discussion

### 6.1. Key contributions

This work presents a systematic method for converting static trusses into reconfigurable, shape-morphing systems using principles of flat-foldable quadrilateral linkages. The key contributions are as follows:

*General rules for node placement that enable reconfigurability in the triangular components of static trusses.* Our proposed method transforms triangular units of static trusses into quadrilateral linkages by introducing an additional node. The node placement is guided by closed-form expressions derived for all triangle geometries (Fig. 1) to satisfy the Grashof flat-foldability criterion in the resulting quadrilateral linkages. These nodes are exclusively placed on tensile members to ensure the structure remains stable under external loads and carries its design load, even with mobility greater than one. Static trusses transformed using this method can be reconfigured to minimize their convex hull area and stored much compactly upon the actuation of their kinematic degrees of freedom.

*A programmatic workflow to transform static trusses into reconfigurable systems and study their kinematic behavior.* We developed a workflow that extends unit-level transformations to the system level. This workflow guides the selection of the candidate members based on the geometry of the triangular units and their member forces in most statically determinate trusses with a continuous series of triangular units between the top and bottom chords. We demonstrate the applicability of our workflow with the help of three commonly observed truss designs (Scissor, Fink, and Warren) and trusses of arbitrary geometries obtained from topology optimization (cantilever, L-shaped, and Serpentine). Additionally, we developed a sequential kinematic simulator to visualize the motion path of the reconfigurable trusses and evaluate their packing density as they morph into different configurations upon sequential actuation of their kinematic degrees of freedom.

*Fabricating proof-of-concept prototypes to demonstrate structural capacities of reconfigurable trusses.* We validated the feasibility of constructing real-life reconfigurable trusses using our

method by fabricating two proof-of-concept prototypes — a 30 cm reconfigurable cantilever truss and a 3 m Warren truss. Both prototypes employ a joint design strategy that distributes truss members in and out of the plane to ensure desired shape-morphing behavior without member contact or overlap. Load testing of the cantilever trusses confirmed that the reconfigurable truss exhibits force-stable behavior and maintains a peak load capacity and structural stiffness comparable to its static counterparts despite having mobility greater than one. The three-meter-long reconfigurable Warren truss weighing 38 kg supported a peak load of 19 kN, demonstrating the structural capacity and scalability of the proposed designs.

## 6.2. Challenges and considerations for future work

While the reconfigurable trusses introduced in this work offer exciting avenues for designing shape-morphing structures, several challenges must be overcome before translating these designs into practical, life-sized structures. Future research will focus on tackling the following challenges:

*Mitigating structural overlap to optimize packing density.* As the complexity and degrees of freedom for reconfigurable trusses increase, the potential for structural self-overlapping during actuation becomes increasingly evident. This issue is particularly highlighted in the Scissor truss example illustrated in Fig. 3 (a), where the actuation of the third degree of freedom results in portions of the structure overlapping. Real-life truss structures cannot achieve a compact state without providing special provisions for folding mechanisms. For such structures, it is crucial to understand their spatial movement patterns and identify the degrees of freedom whose actuation triggers a self-overlap. Addressing this challenge necessitates future investigation into varied sequences of degree-of-freedom actuation to mitigate structural overlap. Furthermore, automating the distribution of truss members out of the plane and incorporating additional methods for node placement (compressive members) will enhance the feasibility of reconfigurable structures. These practices can be explored to prevent self-overlapping and optimize the ability of the structure to minimize its footprint after shape transformations.

*Handling multi-chord trusses, series of similar triangles and polygons in a bar-linked structure.* The node introduction workflow described in Section 2.3 effectively transforms many com-

monly used truss structures into reconfigurable systems. However, the simplifying assumptions used herein limit its applicability when addressing the following three specialized cases. First, trusses with multiple layers of triangles between their top and bottom chords demand meticulous consideration during node introduction. Adding a new node in these configurations is challenging, as it influences the mobility of adjacent triangular units. If not executed carefully, this modification can lead to incompatible kinematics at the unit level, and structural instability and reduced packing efficiency at the system level. Second, truss structures composed of a sequence of similar triangles, as found in Pratt trusses, present a unique challenge while introducing nodes. These repeating patterns often cause certain triangles to be skipped by the current workflow. Therefore, further adjustments are necessary to ensure that nodes are added appropriately and that the structure achieves the desired reconfigurability. Lastly, trusses for arbitrary geometries derived from topology optimization often exhibit complex forms and include polygons with more than three sides. The current workflow is not equipped to handle such complex structures. Future work can focus on strategies that help simplify the structures and refine the workflow to address such complex cases effectively. Alternatively, topology optimization algorithms can be improved to provide optimal truss designs that can be directly transformed into reconfigurable systems. In addition, graph-theory techniques could also be explored to generalize the design process of reconfigurable trusses.

Addressing the aforementioned research topics will pave the way for the development of reconfigurable trusses that effectively balance structural capacity, stiffness, and stability while enabling shape morphability, facilitating on-demand deployment, and ensuring compact storage.

## 7. Concluding remarks

This paper introduces a new method for transforming a static truss structure into a reconfigurable system capable of rapid deployment and functional use. The method draws inspiration from flat-foldable Grashof quadrilateral linkages to introduce an additional node in each triangular unit of a static truss. We establish general rules to guide node placement based on the member forces and geometry of the triangular units. These rules ensure global system reconfigurability while

maintaining the load capacity and stiffness of the structure to a reasonable extent. We demonstrate the applicability of the proposed method on three commonly observed truss designs — Scissor, Fink, and Warren trusses. Using a sequential kinematic simulator, made available as open-source software, we show that the modified trusses achieve up to a 93% reduction in convex hull area when actuated to 99% across all degrees of freedom. We further explore the versatility of the method by applying it to trusses that were obtained using topology optimization designed for arbitrary geometries, load, and support conditions. Finally, we validate the practicality of the method by fabricating and load-testing two proof-of-concept reconfigurable trusses: a 30 cm long topology-optimized cantilever truss and a three-meter-long Warren truss.

## 8. Data Accessibility

The sequential kinematic simulator used for the simulations in this article is available as an open-source code at: [www.github.com/hardikyp/reconfigurable-trusses](https://www.github.com/hardikyp/reconfigurable-trusses). Further improvements and updates to the code will continue to be made.

## 9. Authors' Contributions

**Hardik Y. Patil:** Methodology, Software, Validation, Formal Analysis, Investigation, Data Curation, Writing — Original Draft, Writing — Review & Editing, Visualization.

**Evgueni T. Filipov:** Conceptualization, Methodology, Validation, Resources, Writing — Review & Editing, Supervision, Project Administration, Funding Acquisition.

All authors gave final approval for publication and agreed to be held accountable for the work performed therein.

## **10. Conflict of Interest Declaration**

The authors declare that they have no known competing financial interests or personal relationships that could have appeared to influence the work reported in this paper.

## **11. Acknowledgement**

We acknowledge support from the National Science Foundation (NSF) Grant Number: 1943723, and the Automotive Research Center (ARC) Cooperative Agreement W56HZV-19-2-0001. The paper reflects the views and opinions of the authors, and not necessarily those of the funding entities. DISTRIBUTION STATEMENT A. Approved for public release; distribution is unlimited. OPSEC9589.

## **References**

- Ario, I., Nakazawa, M., Tanaka, Y., Tanikura, I., Ono, S., 2013. Development of a prototype deployable bridge based on origami skill. *Automation in construction* 32, 104–111.
- Baker, J.E., 1980. An analysis of the bricard linkages. *Mechanism and machine Theory* 15, 267–286.
- Barker, C.R., 1985. A complete classification of planar four-bar linkages. *Mechanism and Machine Theory* 20, 535–554.
- Brouwer, G., 2002. Retractable arch will take center stage in salt lake. *Civil Engineering* 72, 15.
- Chen, Y., You, Z., 2005. Mobile assemblies based on the bennett linkage. *Proceedings of the Royal Society A: Mathematical, Physical and Engineering Sciences* 461, 1229–1245.
- Clough, R.W., 1960. The finite element in plane stress analysis. *Proc. 2<sup>nd</sup> ASCE Confer. On Electric Computation*, 1960 .

Constans, E., Dyer, K.B., 2018. Introduction to mechanism design: With computer applications. CRC Press.

Farshad, M., Isfahanian, D., 1978. Iranian plateau - the homeland of original truss structures. *Journal of the American Oriental Society* 98, 248–250. URL: <http://www.jstor.org/stable/598686>.

García-Mora, C.J., Sánchez-Sánchez, J., 2021. Limitations in the design of deployable structures with straight scissors using identical elements. *International Journal of Solids and Structures* 230, 111171.

Gasparini, D.A., Provost, C., 1989. Early nineteenth century developments in truss design in britain, france and the united states. *Construction history* 5, 21–33.

Giersch, L.R., Knarr, K., 2010. Deployment of a Curved Truss. Technical Report.

Grashof, F., 1883. Theoretische Maschinenlehre: Theorie der Getriebe und der mechanischen Meßinstrumente. volume 2. Voss.

Han, B., Xu, Y., Yao, J., Zheng, D., Li, Y., Zhao, Y., 2019. Design and analysis of a scissors double-ring truss deployable mechanism for space antennas. *Aerospace Science and Technology* 93, 105357.

Hibbeler, R.C., Tan, K.H., 2006. Structural analysis. Pearson Prentice Hall Upper Saddle River.

Hoberman, C., 1991. Radial expansion/retraction truss structures. US Patent 5,024,031.

Kassabian, P., You, Z., Pellegrino, S., 1999. Retractable roof structures. *Proceedings of the Institution of Civil Engineers-Structures and Buildings* 134, 45–56.

Kim, S.I., Kim, Y.Y., 2014. Topology optimization of planar linkage mechanisms. *International Journal for Numerical Methods in Engineering* 98, 265–286.

Kim, T.H., Suh, J.E., Han, J.H., 2021. Deployable truss structure with flat-form storability using scissor-like elements. *Mechanism and Machine Theory* 159, 104252.

- Kiper, G., Söylemez, E., Kişisel, A.Ö., 2008. A family of deployable polygons and polyhedra. *Mechanism and Machine Theory* 43, 627–640.
- Li, Y., Krishnan, S., 2023. Geometric design and optimization of scissor-type deployable structures. *Journal of Building Engineering* 65, 105724.
- Liu, S., Chen, Y., 2009. Myard linkage and its mobile assemblies. *Mechanism and Machine Theory* 44, 1950–1963.
- Liu, Y., Bi, Q., Yue, X., Wu, J., Yang, B., Li, Y., 2022. A review on tensegrity structures-based robots. *Mechanism and Machine Theory* 168, 104571.
- Lum, K., Ng, S., Black, I., 2000. Co2 laser cutting of mdf: 1. determination of process parameter settings. *Optics & laser technology* 32, 67–76.
- Mira, L.A., Thrall, A.P., De Temmerman, N., 2014. Deployable scissor arch for transitional shelters. *Automation in Construction* 43, 123–131.
- Miura, K., 1984. Design and operation of a deployable truss structure, in: NASA. Goddard Space Flight Center The 18th Aerospace Mech. Symp.
- Mushtaq, R.T., Wang, Y., Rehman, M., Khan, A.M., Mia, M., 2020. State-of-the-art and trends in co2 laser cutting of polymeric materials—a review. *Materials* 13, 3839.
- Packman, R., 2005. The rolling bridge, paddington basin. *Structural Engineer* 83.
- Patel, J., Ananthasuresh, G., 2007. A kinematic theory for radially foldable planar linkages. *International journal of solids and structures* 44, 6279–6298.
- Qi, X., Huang, H., Miao, Z., Li, B., Deng, Z., 2017. Design and mobility analysis of large deployable mechanisms based on plane-symmetric bricard linkage. *Journal of Mechanical Design* 139, 022302.
- Ross, R.J., et al., 2010. Wood handbook: wood as an engineering material. USDA Forest Service, Forest Products Laboratory, General Technical Report FPL-GTR-190, 2010: 509 p. 1 v. 190.

- Sigmund, O., Maute, K., 2013. Topology optimization approaches: A comparative review. *Structural and multidisciplinary optimization* 48, 1031–1055.
- Snelson, K.D., 1965. Continuous tension, discontinuous compression structures. US Patent 3,169,611.
- Sofla, A., Elzey, D., Wadley, H., 2009. Shape morphing hinged truss structures. *Smart Materials and Structures* 18, 065012.
- Stolpe, M., 2016. Truss optimization with discrete design variables: a critical review. *Structural and Multidisciplinary Optimization* 53, 349–374.
- Studio, H., 2002. Rolling bridge. Retrieved May 30, 2020.
- Thorne, R., 2017. *Structural Iron and Steel, 1850–1900*. Routledge.
- Tibert, G., 2002. Deployable tensegrity structures for space applications. Ph.D. thesis. KTH.
- Turner, M.J., Clough, R.W., Martin, H.C., Topp, L., 1956. Stiffness and deflection analysis of complex structures. *Journal of the Aeronautical Sciences* 23, 805–823.
- Tyrell Rockafellar, R., 1970. Convex analysis. Princeton mathematical series 28.
- Ullah, Z., Ullah, B., Khan, W., 2022. Proportional topology optimisation with maximum entropy-based meshless method for minimum compliance and stress constrained problems. *Engineering with Computers* 38, 5541–5561.
- Wang, Y., Liu, R., Yang, H., Cong, Q., Guo, H., 2015. Design and deployment analysis of modular deployable structure for large antennas. *Journal of Spacecraft and Rockets* 52, 1101–1111.
- Yao, H., Huang, Y., Ma, W., Liang, L., Zhao, Y., 2023. Dynamic analysis of a large deployable space truss structure considering semi-rigid joints. *Aerospace* 10, 821.
- You, Z., Pellegrino, S., 1997. Foldable bar structures. *International Journal of Solids and Structures* 34, 1825–1847.

Zegard, T., Hartz, C., Mazurek, A., Baker, W.F., 2020. Advancing building engineering through structural and topology optimization. *Structural and Multidisciplinary Optimization* 62, 915–935.

Zegard, T., Paulino, G.H., 2014. Grand—ground structure based topology optimization for arbitrary 2d domains using matlab. *Structural and Multidisciplinary Optimization* 50, 861–882.

## Appendix A. Sequential kinematic simulation of multi-DOF reconfigurable trusses

This section outlines the method for developing a sequential kinematic simulation program (attached as Supplementary Material), which enables the movement of one degree of freedom at a time in any reconfigurable truss generated by the workflow in Section 2.3. The reconfigurable trusses in this study consist of two types of units, each with a single degree of freedom (DOF): (*i*) a Grashof quadrilateral linkage; and (*ii*) a unique configuration of a six-bar linkage. The kinematic simulator performs the position analysis of one DOF at a time, while applying rigid rotation and translation to the structure excluding DOFs that were actuated in previous steps. The position analysis for the two types of units is performed as follows.

### A.1. Position analysis of a general quadrilateral linkage

The Method of Projections (Constans and Dyer, 2018, Ch. 4) is used to obtain the position of the nodes of a general quadrilateral linkage, as shown in Fig. A.1 (a-b). For a general quadrilateral linkage,  $\theta_2$  is the known angle made by the input link  $AB$  of length  $a$ . Link  $BC$  is the coupler link of length  $b$  and makes the angle  $\theta_3$  with the horizontal. Link  $CD$  is the output link of length  $c$  and makes the angle  $\theta_4$  with the horizontal. Link  $AD$  is the ground link with length  $d$  and is collinear with the X-axis (horizontal). The objective of the Method of Projection is to find the angles  $\theta_3$ ,  $\theta_4$ , and coordinates of nodes  $B$  and  $C$ , given  $\theta_2$ ,  $a$ ,  $b$ ,  $c$ , and  $d$ .

In Fig. A.1 (a),  $f$  denotes the prime diagonal of the quadrilateral linkage and  $\delta$  is the angle opposite to  $\theta_2$ . The lengths  $r$  and  $s$  are determined using the projections of  $a$  as follows

$$r = d - a \cos \theta_2 , \quad (\text{A.1})$$

$$s = a \sin \theta_2 . \quad (\text{A.2})$$

Using Pythagoras' Theorem, we note that

$$f^2 = r^2 + s^2 . \quad (\text{A.3})$$

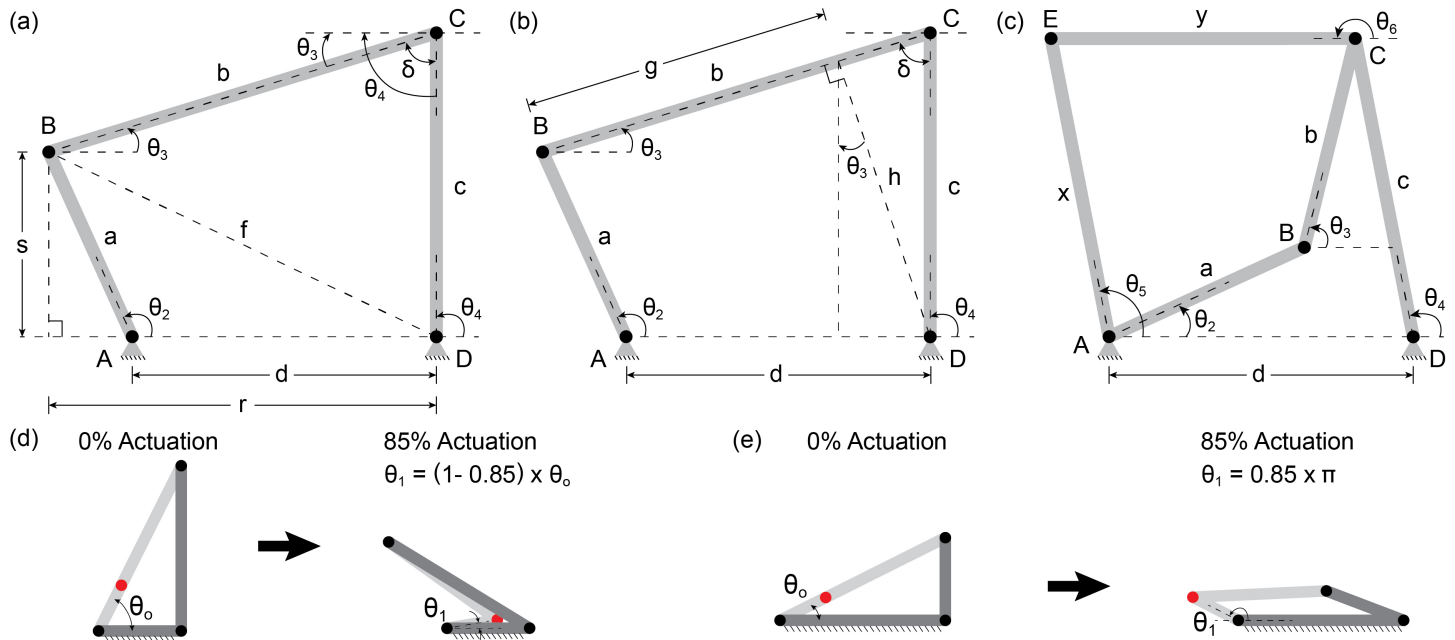


**Fig. A.1.** Position analysis using the Method of Projections for: (a-b) a general quadrilateral linkage; (c) a unique configuration of a six-bar linkage; (d-e) Extent of actuation in terms of % actuation of the DOF explained for two different geometries of quadrilateral linkage. **Note:** A Ground link is not explicitly shown in (a)-(c) but is assumed to be present between nodes A and D.

From  $\triangle BCD$ , we also have

$$f^2 = b^2 + c^2 - 2ad \cos \delta , \quad (\text{A.4})$$

$$\theta_4 = \theta_3 + \delta . \quad (\text{A.5})$$

Simplifying Eq. A.3 and Eq. A.5 yields

$$\delta = \cos^{-1} \left( \frac{b^2 + c^2 - r^2 - s^2}{2bc} \right) . \quad (\text{A.6})$$

Now consider the same quadrilateral linkage, as shown in Fig. A.1 (b). Here, we use  $\delta$  and projections of  $c$  to find the lengths  $g$  and  $h$  as follows

$$h = c \sin \delta , \quad (\text{A.7})$$

$$g = b - c \cos \delta . \quad (\text{A.8})$$

Expressing  $r$  and  $s$  in terms of  $h$  and  $g$ , we get

$$\begin{aligned} r &= g \cos \theta_3 + h \sin \theta_3 , \\ s &= h \cos \theta_3 - g \sin \theta_3 . \end{aligned} \quad (\text{A.9})$$

Simplifying further yields

$$\theta_3 = \tan^{-1} \left( \frac{hr - gs}{gr + hs} \right) . \quad (\text{A.10})$$

With  $\theta_3$  known, we can now calculate  $\theta_4$ , giving us sufficient information to determine the coordinates of each node relative to  $A$  (or the local origin) as well as use  $\theta_4$  to apply rigid rotation to the remainder of the structure. Points  $A$  and  $D$  remain fixed (as they are the ends of the ground link).

The coordinates of  $B$  are determined as follows

$$\begin{aligned} B_x &= A_x + a \cos \theta_2 , \\ B_y &= A_y + a \sin \theta_2 . \end{aligned} \quad (\text{A.11})$$

Similarly, the coordinates of  $C$  are given by

$$\begin{aligned} C_x &= D_x + c \cos \theta_4 , \\ C_y &= D_y + c \sin \theta_4 . \end{aligned} \quad - (\text{A.12})$$

### A.2. Position analysis of 6 bar linkage with a single degree of freedom

The second type of unit observed in the reconfigurable trusses of this study is the 6-bar linkage with exactly one degree of freedom, as illustrated in Fig. A.1 (c). This type of linkage is formed when the two adjacent triangles are congruent and an additional node is introduced on the side shared by the two triangles. In this case, the objective is to find coordinates of  $B$ ,  $C$ , and  $E$ , and angles  $\theta_3$ ,  $\theta_4$ ,  $\theta_5$ , and  $\theta_6$ , given  $\theta_2$ ,  $a$ ,  $b$ ,  $c$ ,  $d$ ,  $x$ , and  $y$ .

The analysis to obtain the coordinates of  $B$  and  $C$ , and angles  $\theta_3$  and  $\theta_4$  is identical to that performed in Appendix A.1. The coordinates of  $E$  are obtained by solving the following equations simultaneously, numerically.

$$(E_x - A_x)^2 + (E_y - A_y)^2 - x^2 = 0 \quad (\text{A.13})$$

$$(E_x - C_x)^2 + (E_y - C_y)^2 - y^2 = 0 \quad (\text{A.14})$$

There are two possible solutions for the above equations. We ensure the correctness of the solution by providing an initial guess for the coordinates  $E_x$  and  $E_y$  — coordinate location of  $E$  in the previous step of the simulation. With the coordinates of  $E$  known, we can determine angles  $\theta_5$  and  $\theta_6$ . These angles, in addition to the displacement of  $C$  provide us enough information to determine the rigid rotation and translation that must be applied to the remaining structure, depending on the side the structure is connected to.

### A.3. A note on the extent of actuation of a quadrilateral linkage

In the sequential kinematic simulator, users can specify the extent of actuation for each DOF. The 0% actuation state represents the initial configuration, while the 100% actuation state corresponds to the flat-folded configuration of the quadrilateral linkage. At 0% actuation of the quadrilateral linkage, the decomposed links of the Candidate link are collinear, as shown in Fig. A.1 (d) and (e) on the left side. In this state,  $\theta_o$  represents the angle between the shorter decomposed link and the Ground link. The transition to the flat-folded or 100% actuation state depends on the geometry of the linkage. The shorter link may rotate in either a clockwise or counterclockwise direction to achieve a flat-folded configuration. In the first case, the shorter link rotates clockwise

until it makes an angle of  $0^\circ$  relative to the Ground link. For an intermediate state of 85% actuation, the shorter link is rotated to an angle of  $\theta_1 = (1 - 0.85) \times \theta_o$  relative to the Ground link as shown in Fig. A.1 (d, right). In the second case, the shorter link rotates anti-clockwise until it makes an angle of  $180^\circ$  relative to the Ground link. For an intermediate state of 85% actuation, the shorter link is rotated to an angle of  $\theta_1 = 0.85 \times \pi$  relative to the Ground link, as shown in Fig. A.1 (e, right).